DELTA UNIVERSITY
SCIENTIFIC JOURNAL
Journal home page: www.deltauniv.edu.eg/dusj

STRENGTHENING OF PRESTRESSED CONCRETE BOX BRIDGE AFTER FIRE EXPOSURE

Xuzheng Liu[1] , Chenxi Yu[1], Wei Quan[2], Liang Chen[3]

1 School of Civil Engineering AND Architecture, EAST CHINA JIAOTONG University, NANCHANG, CHINA

2 School of Civil Engineering AND Architecture, HUANGSHAN University, HUANGSHAN, CHINA

3 HANGZHOU Guotong TRANSPORTATION Science & Technology CORPORATION, HANGZHOU, CHINA

A b s t r a c t

This paper presents inspection, materials testing, field testing and parametric finite element analysis of a pre- stressed concrete box girder bridge after fire exposure. A detailed inspection of the fire-exposed bridge was performed through visual checking, photo examinations, and hammer detection. Samples of the concrete cores and reinforcing bars were tested; the residual strengths of the building materials (concrete, reinforcing bars and prestressed strands) were estimated. Furthermore, the temperatures at various depths were estimated. The data from field studies were used to validate finite element models. The structural behaviors of the original bridge prior to fire exposure were obtained via instrumentation from a reference bridge not exposed to fire. The static proof load test deflection results indicate that the stiffness decreased by approximately 23% after fire exposure and no longer satisfied the design requirement. The measured fundamental frequency of the fire-exposed span was approximately 97% of that of the original span and the theoretical fundamental frequency, indicating that the fire had little influence on the frequency of the concrete structure. Based on this work, the repair requirements of the bridge were determined and undertaken, and the repairs were proven to be effective via a field loading test after strengthening.

Keywords: Bridge fires, Prestressed concrete box girder bridge Materials testing, Finite element analysis Field loading test

1. Introduction

Fire is one of the most common and costly hazards to which built infrastructures may be subjected during their service life. Numerous bridge fire accidents have occurred in recent years with the rapid de- velopments in ground transportation.

Bridge fires lead to significant economic and public losses to the affected region. Because bridges are always built at traffic junctions or over obstacles, such as valleys, railways or rivers, traffic on fire-damaged bridges often cannot easily be detoured. Furthermore, a severe fire may cause permanent

damage to or the complete failure of bridge elements. As a result, it may cost large amounts of money, time and labor to repair a fire-damaged bridge or build a new one.

According to a survey of the positions of previous bridge fires, there are two common fire sites: on the bridge deck and below the bridge span. When vehicles carrying hazardous materials (such as flammable or spontaneously combustible materials) travel on a bridge deck, they can be regarded as potential fire dangers. For example, Fig. 1 shows a fire caused by a coal truck on the Barlin River bridge at mile 1985 of the G60 freeway in Guizhou Province, China. Fire hazards can also occur

Fig. 1. Fire accident on a bridge deck.

Fig. 2. Fire below the bridge span.

below bridge spans. Fig. 2 shows a fire caused by an accident involving a fireworks truck below an overpass span that broke out at the Daqi Road/G4 Expressway interchange near Hebi City in Henan Province, China. Additionally, some Chinese urban residents store flammable sundries, such as timber or straw, below bridge spans for use as shelters, and these materials have been one of the major causes of bridge fires. A fire can damage a bridge to different extents according to the fire's position and the properties of the fire [1–4].

Fire damage to a bridge is highly dependent on the building mate- rials used to construct the bridge. The influence of a given fire scenario on the structural performance of a concrete bridge is less than that on the structural performance of a steel bridge because concrete has a better fire-resistance performance than that of steel. Currently, there are approximately 800,000 bridges in the highway transportation system in China. Less than 0.3% of these bridges are steel bridges (in- cluding steel-concrete composite bridges) [5,6]. This low percentage can be attributed to the high investment costs, high maintenance costs and high dependency on heavy mechanization of steel bridges. Nearly all bridge fires have occurred near concrete bridges in China [7]. However, few of these fires resulted in the complete collapse of the

bridge. The vast majority of the concrete bridges experienced various extents of damage during the fire exposure, but no collapse occurred. In these cases, the following tasks must be performed on the fire-exposed bridge: (1) inspect the fire-induced damage, (2) evaluate the residual strength of the fire-exposed bridge, and (3) determine the repair stra- tegies.

A review of the literature indicates that there is a lack of published standards or criteria for the inspection, assessment and repair methods for postfire concrete bridges. However, an increasing number of studies have sought to increase the awareness of the tremendous social and economic consequences of fire damage to bridges. CECS 252 [8] is a standard for building structural assessments after a fire enacted by the China Association for Engineering Construction Standardization (CECS). This standard specifies the investigation and test methods, structural analysis methods, element inspection and assessment ranking of structural elements. Although this standard is applicable to postfire buildings, some provisions and guidelines, such as those regarding the

properties of materials after cooling, can also be applied to postfire concrete bridges. NCHRP report 280 [9], PCI Manual 124 [10], and Fib Bulletin 46 [11] can be used as the bases for the assessment and repair strategies of postfire concrete bridges. These references provide certain guidelines, including those for the evaluation of the concrete residual strength, the estimation of the temperature history of the areas of the bridge based on the fire scenario, and repair strategies for fire-damaged concrete bridge elements depending on the type of damage [12].

Georgali and Tsakiridis [13] inspected the microstructure of fire- damaged concrete. Short et al. [14] studied color images of fire-da- maged concrete with optical microscopy. Kodur et al. [15,16] analyti- cally and experimentally studied the critical factors governing the re- sidual strength of postfire reinforced concrete beams using Abaqus. Lu et al. [17] analyzed the mechanical performance of fire-damaged con- tinuous reinforcement concrete (RC) beams using a numerical ap- proach. Huang [18] experimentally studied an RC box beam bridge under fire exposure via inspection, materials testing and a field loading test. With regard to a fire-damaged prestressed concrete bridge, the concrete, prestressed strands and mild steel reinforcement might suffer losses of strength and stiffness upon exposure to high temperatures. Guyon [19] first reported the loss of tensile strength of strands pre- stressed under high temperatures. The PCI Manual [10] provides gui- dance on the residual strength of strands for temperatures ranging from less than 400 °C–600 °C. Davis et al. [20] assessed the damage to a precast, prestressed concrete bridge caused by a tanker accident and fire. Stoddard [21] presented a detailed inspection and repair of a fire- damaged prestressed girder bridge. Garlock et al. and Cai et al. [22] evaluated the residual strength of a 30-m-long prestressed box beam under fire exposure through visible inspection, experimental testing, and structural dynamic testing. Liu et al. [23] assessed a postfire pre- stressed concrete hollow slab girder via simulations of the fluid-solid coupling heat transfer model of a hollow slab of concrete with air in its closed cavity. Bruno et al. diagnosed a fired steel bridge.

In the majority of research studies on postfire bridges, the fire im- pact on the structural strength is determined by theoretical results from a finite element method or experimental data from postfire bridge field tests [24–26]. Regardless of which approach is taken, the original structural performance of the bridge prior to the fire exposure cannot be obtained accurately. The theoretical structural performance calculated according to the initial design parameters is usually assumed to be the original structural performance prior to the fire exposure. However, the actual structural performance is lower than the theoretical structural performance due to deterioration;

thus, the impact of the fire on the bridge is likely to be incorrectly assessed. To address this issue, this paper studies the influence of fire on a prestressed concrete bridge by comparing the original structure prior to the fire exposure and the postfire structure. The fire-damaged S12 bridge, shown in Fig. 3, was composed of some continuous units. With regard to continuous unit 1 (fired bridge), the material

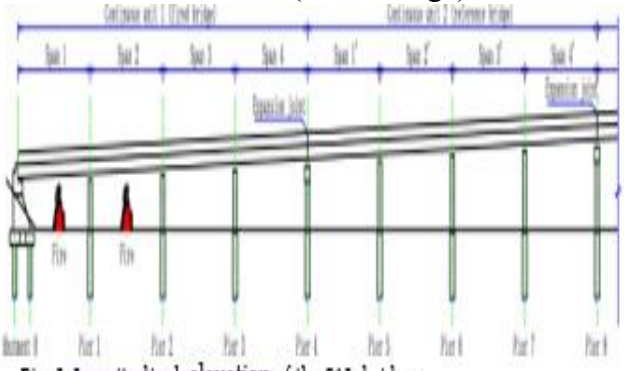

Fig. 3. Longitudinal elevation of the S12 bridge.

bridge has the same design, construction and working conditions as those of the fired bridge. Therefore, the reference bridge has the same structural behaviors as did the original bridge prior to the fire exposure. Thus, the degradation of the structural performance of the bridge after fire exposure can be precisely studied by testing the reference and fired bridges in the field.

The goal of this study is to investigate a prestressed concrete box girder after fire exposure. The study includes inspection, materials testing, field testing and parametric finite element analysis. A detailed inspection of the fire-exposed bridge was performed through visual assessments, photo examinations and hammer detection. Material samples of the concrete core and reinforcing bars were tested in a la- boratory. In addition, the elevated temperatures at various depths of the S12 bridge elements were estimated. Data from field studies, in- cluding static and dynamic testing, were used to validate the computer models with Midas

degradation of spans 1 and 2, which were subjected to fire damage, will affect the other spans in the continuous unit. Thus, the spans located in the same continuous unit should not be employed to ascertain the original structural performance. Rather, spans of continuous unit 2 (reference bridge) adjacent to continuous unit 1, which was not affected by the fire, is selected. The reference

software. In particular, the structural behaviors of the original bridge prior to fire exposure were obtained via in- strumentation from a reference bridge that was not exposed to fire. The results of this paper can be used to determine the structural perfor- mance of a prestressed concrete box girder bridge after fire exposure and provide subsequent suggestions for postfire bridge strengthening.

1.1. *Fire DAMAGE to the S12 bridge*

The S12 bridge, shown in Fig. 4, is a continuous prestressed con- crete box girder bridge located on the S12 expressway at km 61.479 in Zhejiang Province, China. The S12 bridge consists of twenty spans, with every four spans combined into a continuous unit. The total length of the bridge is 500 m, with a constant span length of 25 m. Fig. 5 depicts a typical cross section with inclined webs, consisting of a simple box with double cells. The constant depth of the beam is 1.4 m, and the total width is 12 m, with 2-m-wide flanges on both sides. The thicknesses of the top slab and bottom slab are 25 and 20 cm, respectively. The con- crete box girder is prestressed longitudinally and transversely with prestressing tendons. These tendons are made of Φ15.24 mm seven- wire strands with an ultimate strength of 1860 MPa. Tendons N7, N8 and N9 are set in three box webs. The bridge was completed in 2006 and was in service for over ten years before the fire accident [27].

At approximately 2 a.m. on Friday, July 31, 2015, a fire accident on the S12 overpass was

reported by highway patrols. The fire lasted approximately 2 h before firefighters approached and extinguished it with water at 4 a.m. According to the investigation results, the fire began in the textile wastes that were piled up below one span and propagated to nearby scrap wood below an adjacent span; however, the cause of the fire remains unclear. The vertical clearance below spans 1 and 2 is approximately 4 m. According to the extents of burning embers below the spans, the fire-affected area below each span is approximately 6 × 15 m^2. The fire accident damaged the bridge elements, i.e., the

beams, columns and bearings, to various extents. The CHD Engineering Center, Inc., arrived at the fire site at 7 a.m. on the same day and performed a fire damage inspection. According to the results of the initial inspection, the S12 bridge was partially damaged by the fire, and the structural performance of the bridge was thought to have possibly decreased after the fire exposure. Therefore, the S12 bridge was immediately closed to traffic, and detour roads were soon arranged.

Fig. 4. Fire-damaged S12 bridge.

2. Inspection, materials testing and fire effect analysis

2.1. *Inspection*

A detailed inspection of the S12 bridge was performed by CHD Engineering Center, Inc., in July 2015. The inspection involved visual and photo examinations of the beams, columns, abutments and deck. These fire-affected areas were also sounded with a hammer to detect locations of delamination in the concrete. Furthermore, some damaged concrete covers were removed with an electric drill to check the in- ternal concrete and bar conditions. The locations of concrete spalling, loss of concrete cover, prestressed tendons, excessive cracking and concrete discoloration were documented in detail.

The fire damage patterns indicated that the fire-damaged portions were mainly within span 1 (Fig. 6) and span 2 (Fig. 7). The typical damage on abutment 0 was soot on the front-wall surface and a light pink color and map cracking on parts of the surface concrete. No con- crete spalling was observed on the abutment elements. The fire damage to the beam elements is summarized in Table 1, and a schematic of the damage to the spans is plotted in Fig. 8.

Four piers were observed to be clearly damaged by fire to various extents. The most severely damaged pier appeared white-gray in color in the local concrete area, with rough map cracking in 60% of the area, local concrete spalling and visible traces after hammering. The abut- ment concrete appeared light pink in color. All bearings were checked, and no visible damage was observed, except for partial coating loss in the steel component. Additionally, as shown in Fig. 9, the deck showed obvious reinforcement exposure in the fire-affected area.

2.2. *Materials testing*

The residual strengths of the building materials, including the concrete, reinforcing bars and strands, are vital to the structural performance of a bridge that experienced fire exposure. Material samples were tested by an independent testing laboratory. The samples of

the concrete core and reinforcing bar were taken from the most severely damaged areas to provide a conservative strength estimate.

The reduction coefficients of the postfire concrete compressive strength under various surface temperatures are suggested in CECS 252 [8] and shown in Table 2. The data are applicable only to the water cooling-down method. Due to the complexity of fire scenarios, the re- commended reduction coefficient does not agree with the practical postfire concrete strength in certain cases. Hence, the postfire concrete compressive strength was tested by the resiliometer method in the field, as well as by core compressive testing in the laboratory. With regard to the resiliometer method, the calibration curve used to estimate the compressive strength of unheated concrete should not be adopted for postfire concrete, as the postfire concrete was dried by fire. Therefore, the concrete compressive strength was estimated by sampling core testing instead of by the resiliometer method. The sampling cores were taken from a depth of more than 5 cm under the concrete surface to avoid the influence of surface concrete spalling and cracking. In addi- tion, three sampling cores of corresponding elements were taken from areas not affected by the fire as references. The concrete reference compressive strength and the postfire compressive strength are listed in Table 3.

A postfire concrete sample taken from a depth of 5 cm was also checked via petrographic examination to distinguish the damage extent

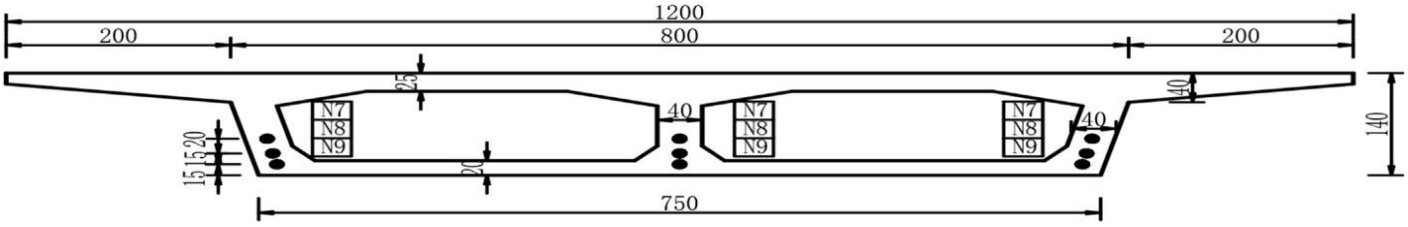

Fig. 6. Fire-damaged span 1.

Fig. 7. Fire-damaged span 2.

and property changes of the heated concrete, i.e., the depth of micro- cracking, paste alteration (color change and strength softening) and carbonation. The temperatures at various depths of the inner concrete can be estimated according to the petrographic examination results obtained using an electron microscope. CECS 252 [8] suggests the changes in the microcharacteristics of concrete corresponding to var- ious temperature ranges. Fig. 10 a) shows a petrographic picture taken from a depth of 5 cm from the concrete surface in a postfire beam. The color of the sampling was white-gray, the cement remained tense with good integrity, and no microcracking was found. According to a com- parison of the petrographic results with CECS 252 [8], the temperature of the concrete at a depth of 5 cm was estimated to range from 350 °C to 550 °C during the fire. Fig. 10 b) shows the original concrete surface unexposed to fire.

The reduction coefficients of the postfire

reinforcing bar tensile strength under various exposed temperatures are summarized in Table 4 from CECS 252 [8]. Following the recommended assessment method, three segments of the HRB335-type reinforcing bar with a 16 mm diameter were taken from the soffit (Fig. 11) and tested via

tensile tests (Fig. 12) to ascertain the postfire bar tensile strength. Ac- cording to the test results, the minimum yield strength of the postfire bar was 348.3 MPa. In addition, the initial records of the bar in the construction stage were checked, and the recorded original minimum yield strength of an HRB335 bar with a 16 mm diameter was
412.5 MPa. Hence, the calculated reduction coefficient of the bar was approximately 0.85, which corresponds to the recommended value at 700 °C. This result indicates that the temperature of the testing bar reached 700 °C during the fire exposure. Because the concrete cover spalled off during the fire, the sampled segments of the reinforcing bar were exposed. Accordingly, it is inferred that the beam surface tem- perature reached 700 °C during the fire.

Prestressed strands have a proven loss of tensile strength and stiff- ness after suffering high temperatures. Abrams and Erlin [28] found that the residual tensile strength after 8 h of fire exposure remained at 90%, 60%, 41%, 32% and 29% at temperatures of 400 °C, 500 °C, 600 °C, 704 °C and 865 °C, respectively. The PCI Manual [10] re- commends that the residual prestressed strand strengths be 100%, 70% and 50% at the temperature ranges of less than 400 °C, 400–482 °C and 482–600 °C, respectively, after heating and cooling. In this fire acci- dent, the temperature data of the prestressed strands cannot easily be obtained directly, but they can be estimated according to the corru- gated pipe status after the fire exposure. Part of the corrugated pipe of web tendon N9 (see Fig. 5), which is located at the lowest position of the prestressed tendons, was removed and tested in the laboratory. The material of the corrugated pipe was determined to be polypropylene (PP). A chemical composition analysis indicated that thermal decom- position of the PP materials did not occur, which indicates that the temperature of the corrugated pipe was lower than the decomposition temperature of the PP material during the fire exposure. However, the pattern on the surface of the corrugated pipe was blurred and melted, which indicates that the temperature of the corrugated pipe was higher than the melting point of the PP material during the fire exposure. Due to the presence of oxygen, the melting point and decomposition tem- perature of PP in an aerobic environment are slightly lower than those in an anaerobic environment. As the corrugated pipe was inside the concrete during the fire exposure, the temperature of the corrugated pipe ranged from 190 °C to 390 °C, corresponding to the melting point and decomposition temperatures of PP in an anaerobic environment, respectively. According to the estimated temperature of the corrugated pipe during the fire exposure, the conservative prestressing of tendon N9 was estimated to retain 90% of the room-temperature prestressing, and the other tendons, i.e., N7 and N8, retained all of the prestressing.

2.3. *Elevated temperature estimation*

The residual loading capacities of postfire bridges are determined by many factors, such as the fire type and duration, extinguishing method and fire damage level. The thermal distribution of the bridge span and elevated temperatures of the bridge elements during the fire exposure are also important in estimating the residual strength of the postfire bridge. The surface temperature of the bridge elements during fire ex- posure can typically be assessed based on the concrete color, damage level and hammer testing response. Using the heat conduction rules, the theoretical

elevated temperature of the bridge elements during the fire exposure can be estimated based on

the fire process, fire damage level

Table 1
Description of the damage to the beam elements.

Span	Element	Damage description
span 1	right flange	Soot throughout the span, pink in the midspan ranging from 9.3 to 16.8 m, map cracking in 80% of the area with a crack width of less than 0.15 mm, cover loss in certain areas.
	right web	White-gray color ranging from midspan to pier 1, soot adjacent to abutment 0 and pink in the transition zone, rough map cracking in 40% of the area, clear concrete spalling ranging from 8.6 to 17.2 m, a maximum gap depth of 4.3 cm, and reinforcement exposed near the soffit.
	soffit	White-gray color ranging from midspan to pier 1, soot adjacent to abutment 0 and pink in the transition area, rough map cracking in 40% of the area, significant concrete spalling ranging from 3.8 to 23.8 m, a maximum gap depth of 4.3 cm, and reinforcement exposed in the area corresponding to the middle web.
	left web	Soot throughout the span, white-gray color in the midspan near the soffit, local rough map cracking, concrete spalling ranging from 5.6 to 15.6 m, a maximum gap depth of 3.5 cm, and reinforcement exposed near the soffit.
	left flange	Soot throughout the span, no clear cracking, spalling or cover loss.
	others	The bottom corrugated pipe in the right web was exposed with a drill, and the pipe shape remains. The pattern on the surface was blurred and melted. Part of the corrugated pipes of the web tendon in the severely damaged area, located 15 cm from the bottom and 19.4 cm from the edge of the right web, was removed and tested in the laboratory, and the testing results are provided in subsequent sections.
span 2	right flange	Soot throughout the majority of the span, pink within 5 m located at L/4, map cracking in these areas, and a crack width of less than 0.15 mm.
	right web	Soot throughout the span, white-gray color near L/4, pink in the transition area, rough map cracking in 10% of the area, significant concrete spalling ranging from 9.6 to 15.7 m, and a maximum gap depth of 3.5 cm.
	soffit	Soot throughout the span, white-gray color near L/4, pink in the transition zone, rough map cracking in 15% of the area, local concrete spalling ranging from 9.6 to 15.7 m and 5–10.8 m on the left side and from 4 to 10.4 m in the middle area, with a maximum gap depth of 5.5 cm.
	left web	Soot throughout the span, white-gray color near L/4, pink in the transition area, rough map cracking in 15% of the area, local concrete spalling ranging from 5.0 to 10.8 m, a maximum gap depth of 3.5 cm, and no reinforcement exposed.
	left flange	Soot throughout the span, no clear cracking, spalling or cover loss.
	others	In part of bar in the severely damaged area located at L/4 corresponding to the position of the middle web, the surrounding concrete was removed, and the bond with the reinforcement remained good.

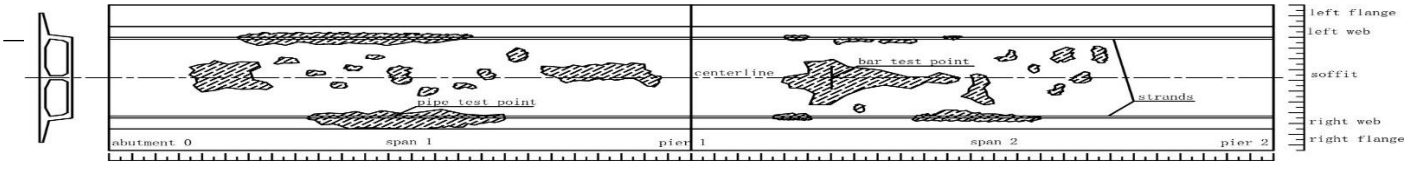

Fig. 8. Schematic of the fire-damaged area in the beam.

Table 2
Reduction coefficients of the postfire concrete compressive strength after water cooling.

Temperature /°C	room	300	400	500	600	700	800
reduction coefficient	1.00	0.70	0.60	0.50	0.40	0.25	0.10

Table 3
Compressive strength of concrete sampling cores (from a depth of more than 5 cm) from the S12 bridge.

Element	Concrete grade	Design strength /MPa	Reference strength /MPa	Postfire strength /MPa
beam	C50	50	62.35	58.13
pier	C30	30	38.07	36.46

of the elements and material properties.

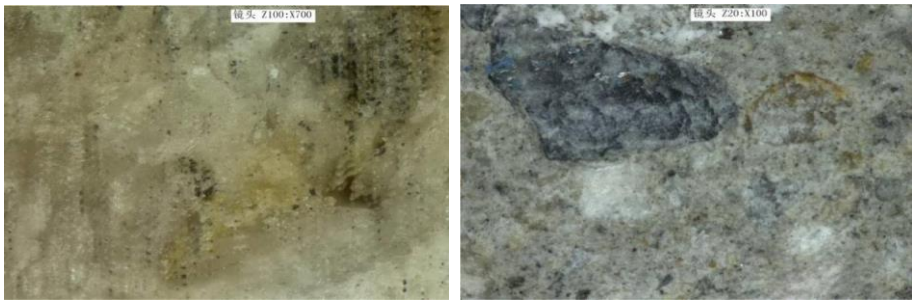

a) Postfire state b) Original state

Fig. 10. Petrographic photographs of various states of concrete.

Table 4
Reduction coefficient of the tensile strength of the postfire HRB335 bar after cooling.

Temperature/°C	Reduction coefficient	
	Yield strength	Ultimate tensile strength
room	1.00	1.00
100	0.95	1.00
200	0.95	1.00
250	0.95	0.95
300	0.95	0.95
350	0.95	0.95
400	0.95	0.90
450	0.90	0.90
500	0.90	0.90
600	0.90	0.85
700	0.85	0.85
800	0.85	0.85
900	0.80	0.80

Fig. 11. Bar sample from the soffit.

maximum surface temperature of the beam and pier during the fire exposure exceeded 700 °C, and the abutment reached a temperature over 500 °C.

The thermal distribution of the concrete building elements during a fire can be determined with CECS 252 [8] or BS EN 1992:1–2 [31]. Due to the openness of the environment during a bridge fire, the tempera- ture-distance relative graphs of the

Table 5
Estimated temperatures at various depths of the S12 bridge elements.

Element	Depth/cm	Temperature/°C
beam	0–2	700–750
	2–4	550–700
	4–7	350–550
	7–10	200–350
	10–14	< 200
column	0–2	650–700
	2–4	500–650
	4–6	300–500
	6–8	< 300
abutment	0–2	550–600

3. Field load testing

bridge elements are very different from those of building elements. Based

According to the previous inspection results, the concrete surface color in the most severely fire-affected area, mainly the webs and soffits of the beams and pier columns, was white-gray, and the abutment concrete exhibited a light pink color. The fire-exposed concrete was

observed to have clear damage, e.g., spalling,

cracking and cover loss. In addition, the concrete was observed to be friable and sounded heavy during the hammer impact tests in the fire-exposed area. In conclusion, with reference to the research results of Stoddard [21] and Glasheen [29], the PCI report [30] and the CECS 252 standard [8], the estimatedupon previous inspection re- sults, the conservatively estimated temperatures of various depths of the S12 bridge elements during fire exposure are summarized in Table 5. Additionally, the estimated elevated temperature can be used to assess the residual strengths of the elements.

3.1. *Testing sections AND INSTRUMENTATION INFORMATION*

Field load testing is a direct approach to ascertain the structural performance of a postfire bridge. Static and dynamic load testing of the fire-exposed bridge was performed by the CHD Engineering Center, Inc., in August 2015. The selected testing sections are illustrated in Fig. 13. Section A (10 m distance from abutment 0) of span 1 and section B (12.5 m distance from pier 1) of span 2 are the critical sections of the four-span continuous bridge under a live load and were instrumented for the load testing. Spans 1 and 2 are also within the range of the fire-affected area. For the purpose of comparison between the postfire span and the original span, section A′ of span 1’ within the second continuous unit was instrumented as a reference for section A of span 1 within the first continuous unit. The locations of the strain gauges and deflection gauges of the testing sections are depicted in Fig. 14. Strain gauges 1, 2 and 3 were installed on the soffit bottom of the box girder, and strain gauges 4 and 5 (instrumented only in section

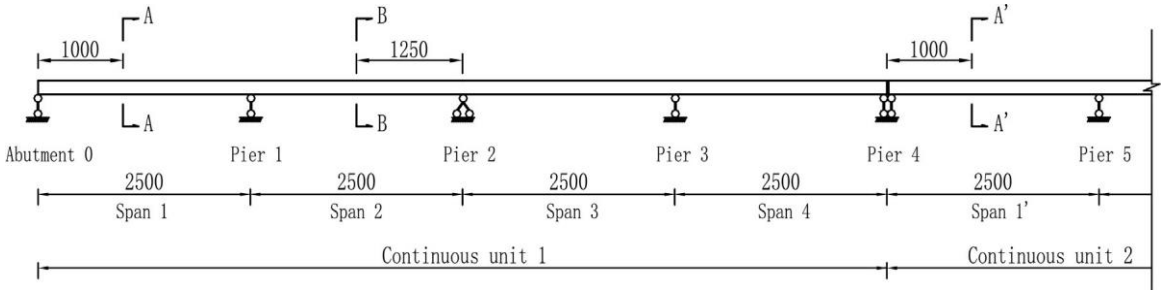

Fig. 13. Instrumentation sections (unit: cm).

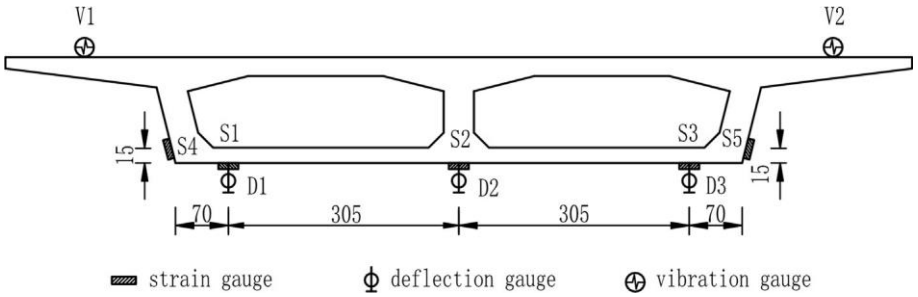

Fig. 14. Gauge locations (unit: cm).

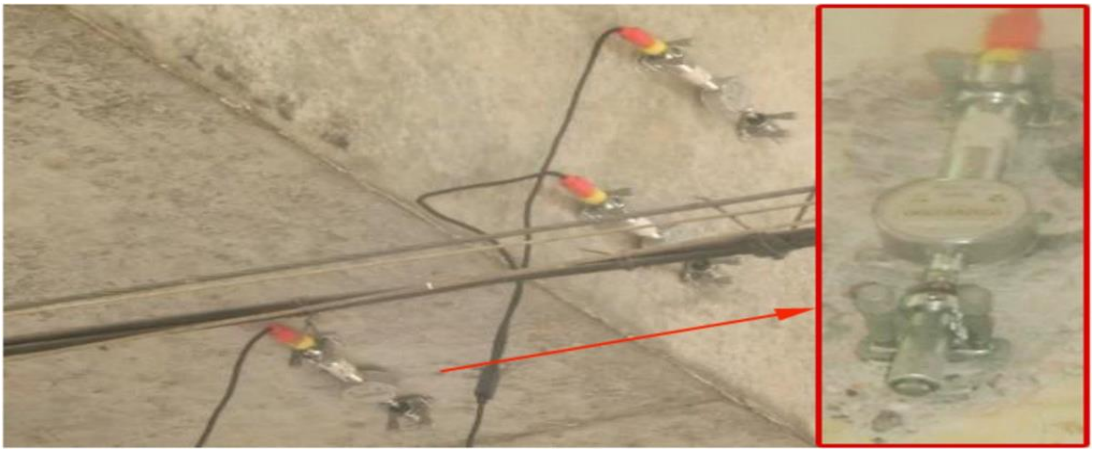

Fig. 15. Installation of the strain gauges.

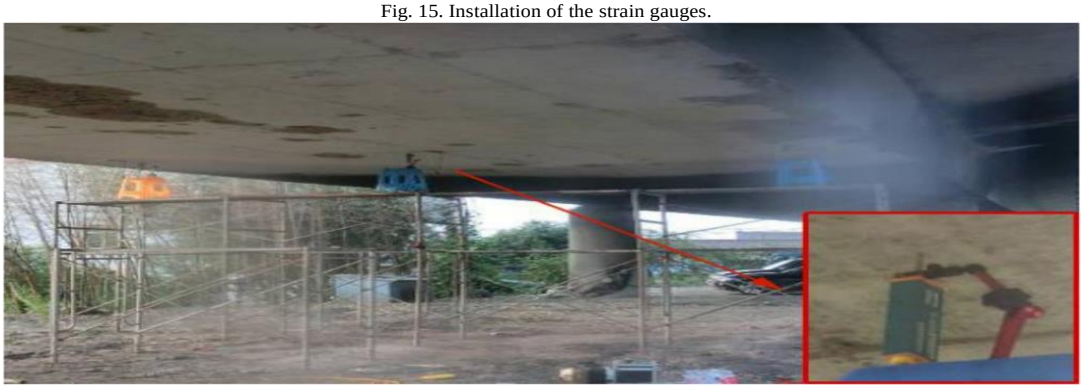

Fig. 16. Installation of the deflection gauges.

A) were installed on the web surface at a depth of 15 cm above the soffit bottom surface. In addition, deflection gauges 1, 2 and 3, with a precision of 0.01 mm, were situated on the soffit bottom surface of the box girder. Vibration gauges 1 and 2 were set on the deck of the test sections to collect the ambient vibration values to analyze the bridge fundamental frequency.

The data quality is of the utmost importance in any experimental field test. In this testing sequence, the equipment was rigorously checked within the laboratory, including the measurement equipment and sensors. Before the gauges were attached, the spalled concrete was removed, and the concrete surface was evened to establish a proper contact surface. Next, the strain gauges were firmly attached to the concrete surface with high-strength glue, as shown in Fig. 15, and the deflection gauges were tightly braced on the soffit bottom surface of the girder with steel brackets, as shown in Fig. 16.

3.2. *Finite element model*

To assess the structural performance of the postfire bridge, finite element models were developed to determine whether the measured responses agreed with the predicted responses under the applied loading. Two different models were established with Midas civil soft- ware, which is software used in bridge engineering. The girder in the FEM models, which employs a three-dimensional beam element, is di- vided into 88 elements and 89 nodes. The girder is supported by four ideal sliding bearings and one ideal hinged bearing. A divided zone method, in accordance with the linear-elastic principle, is applied to consider material degradation, cracking and cross-section weakening. Models A and B represent the original bridge prior to fire exposure and the postfire bridge, respectively. In Model A (unit 2), the parameters of the building materials and dimensions are taken from the original de- sign parameters, whereas Model B (unit 1) employs the parameters of the postfire materials (the compressive strength and elasticity modulus of the concrete, tensile strength of the reinforcing bar and prestressing of tendons) and reduced sizes of the postfire sections.

To develop the fire-damaged Model B, the fire-affected area of the girder was divided into three zones (zones A, B and C) depending on the fire damage level, as shown in Fig. 17. Zone A was observed to have no visible damage except soot on the surface; hence, the material proper- ties and section sizes of zone A were not changed compared with those of Model A. Zone B appeared to have cracking and a light pink color on

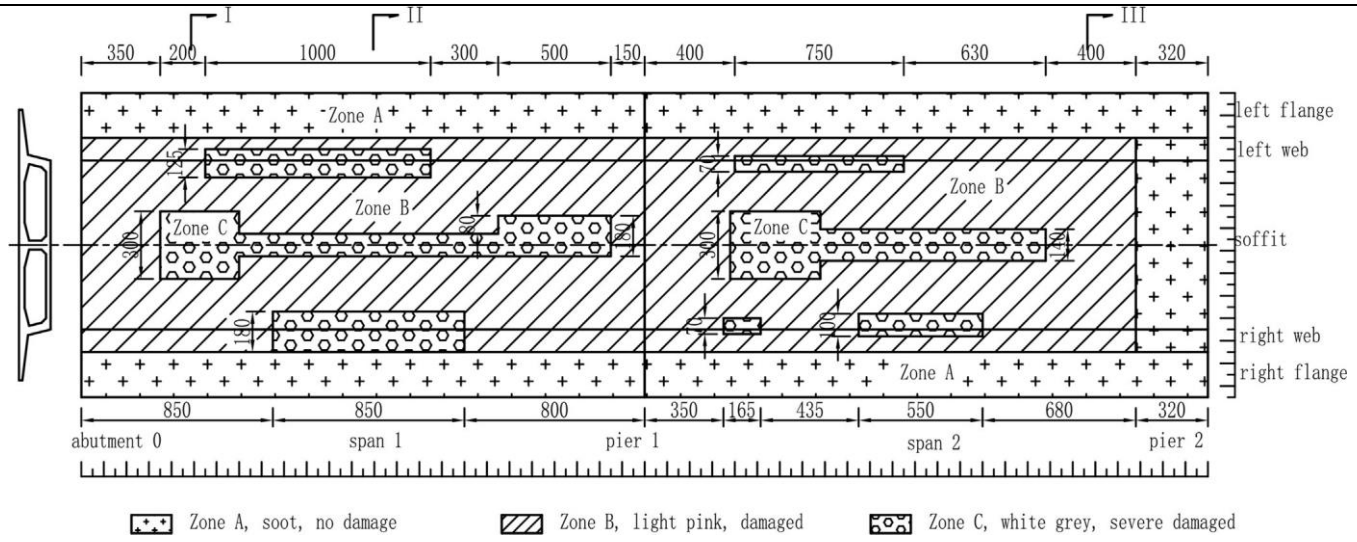

Fig. 17. Divided zones of the fired beam in Model B.

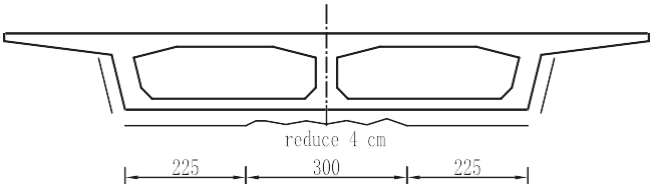

a) Section I

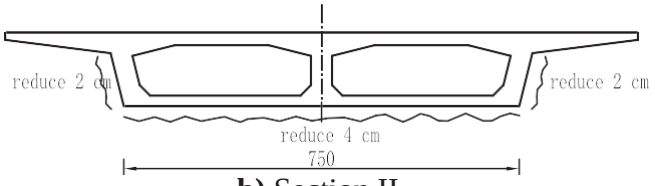

b) Section II

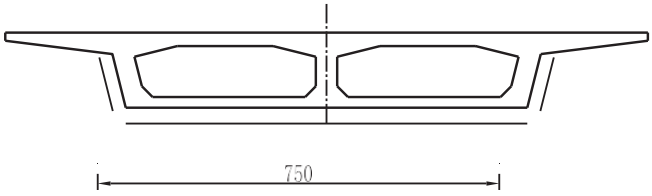

c) Section III

Fig. 18. Reduced sizes of various sections in Model B (unit: cm).

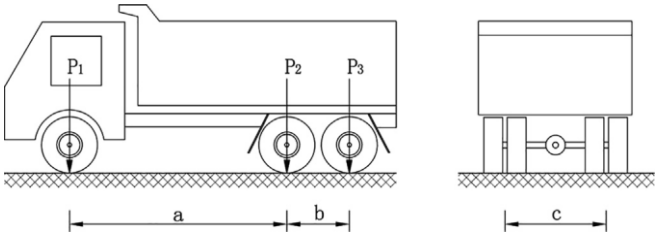

Fig. 19. Schematic of a triaxle truck.

the surface. Due to the degradation of materials by the fire, the material strength properties of zone B were decreased according to the material testing results. Because no clear spalling or cover loss was observed, the section size did not have to be reduced in zone B. Zone C was the most severely fire-damaged area. Hence, both the material strength proper- ties and section size of zone C were reduced. Due to the exposure of the reinforcing bars in zone C, the reduced size of the sections was assumed to be 4 cm, corresponding to the clear cover thickness. Fig. 18 illustrates the reduced sizes of various cross sections. The parameters of different zones in the FEMs are listed in Table 6. The prestressing of the N9 tendons is regarded as retaining 90% of the room-temperature pre-stressing according to the previous results in this paper.

3.3. *STATIC field test*

Load testing provides a method of determining how a real structure actually behaves under applied loading. The aim of the load testing of the postfire bridge is to determine whether the structural behavior is within the linear-elastic range under equivalent design loads and to determine the residual load-carrying capacity. Hence, a proof load test was conducted, and the efficiency of the proof loading was determined by Equation (1) according to Chinese regulations [32]. The load rating

Table 6
Parameters of different zones in the FEM models.

Model	Zone	Concrete compressive strength /MPa	Concrete modulus of elasticity N/mm^2	Bar tensile /MPa	Section size /cm	Strand prestressing /MPa
Model A	All	62	34500	412.5	no change	1395
Model B	Zone A	62	34500	412.5	no change	N9 is 1255.5, others are 1395.
	Zone B	60	32775	382.0	no change	
	Zone C	58	31050	348.3	reduce 4	

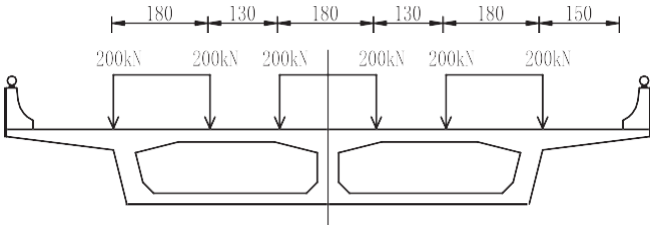

a) Centered

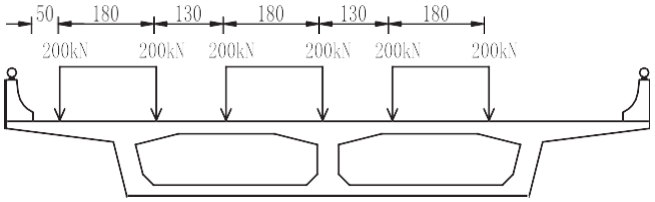

b) Eccentric

Fig. 20. Transverse testing load arrangement (unit: cm).

Fig. 21. Eccentric truck loads in the field.

Table 7
Load efficiency factors.

Test condition	Considered section	S_s/kN m	$\mu\varepsilon$ /kN m	Load efficiency factor
Condition 1	A	4588.1	4445.4	1.032
Condition 2	B	3579.2	3530.9	1.014
Condition 3	A′	4656.7	4445.4	1.048

The design load rating of the S12 bridge is QC-20 grade, and the maximum load is 55 tons, as in the Chinese criterion [33]. To satisfy the load efficiency in the considered sections, four triaxle trucks weighing 40 tons each were placed in assigned positions. Fig. 19 shows a schematic of the triaxle truck. The distances of a, b and c are equal to 4.6 m,
1.4 m and 1.8 m, respectively. The magnitude of P1 is 80 kN, and the magnitudes of P2 and P3 are both 160 kN. Three conditions of the static loading test were carried out in the considered sections, i.e., A, B and A'. To ascertain the transverse structural behaviors of the box girder, each condition contained centered and eccentric truck loads, as shown in Fig. 20 and Fig. 21. Table 7 presents the load efficiency factors of the considered sections as calculated by the moments.

The measured deflection results are summarized in Table 8. The testing coefficient is an important factor indicating the structural behaviors of a practical bridge. If the factor is smaller than 1, it indicates that the practical structural performance is higher than the theoretical structural performance. The value of the relative residual is used to judge whether the structure is in the linear-elastic state during the field tests. It is inferred that the structural behavior is within the linear- elastic range when the value of the relative residual is less than 20% in most cases. The testing coefficients of conditions 1 and 2 are in the ranges of 0.98–1.07 and 0.99–1.06, respectively. The measured deflections are nearly equal to the theoretical deflections in fire-damaged Model B, indicating that the structural behaviors of the theoretical Model B coincide with those of the actual postfire bridge. In addition, the values of the relative residuals are all small, with a maximum value of 5.55%, which indicates that the girder can nearly recover its original position after removing the applied loads. In conclusion, the

postfire bridge is within the linear-elastic condition under the testing loads. Condition 3 was considered in section A′, which was not affected by fire. The testing coefficients of condition 3 varied from 0.82 to 0.89, which indicates that the actual stiffness is larger than the theoretical stiffness in Model A, and the stiffness of span 1' can satisfy the design requirement.

Fig. 22 shows a comparison between the measured deflections and theoretical deflections of sections A and A′ under eccentric and centered testing loads. Under the same eccentric testing loads, the measured deflections of section A were smaller than those of section A'. The measured deflections of D1 (see Fig. 14) in sections A and A′ were 5.289 and 3.879 mm, respectively. Under the same centered testing loads, the average measured deflections in sections A and A' were 4.969 and 3.82 mm, respectively, indicating that the stiffness of span 1 decreased by approximately 23% after fire exposure.

Dividing the elastic value of section A by the theoretical value of section A' (see Table 8) yields values ranging from 1.06 to 1.15, which indicates that the stiffness of span 1 cannot satisfy the stiffness of span 1′ or the design requirement. In addition, the comparison of the testing coefficients between Models A and B can determine whether the di- vided zone method can be used to precisely simulate the fire-exposed span. In other words, if the deflection testing coefficient of section A′ in Model B, which is established by the divided zone method, is in accord with the deflection testing coefficient of section A in Model A, it is in- ferred that the stiffness simulation of the fire-exposed span by the di-

should be set such that permanent damage to the structural integrity and serviceability of the bridge is avoided. Thus, the static test load was applied gradually, and the in situ structural responses were monitored throughout the testing process.

$0.95 \le \eta = \frac{S_S}{} \le 1.05$

Table 8) and 0.82–0.89 (condition 3 in Table 8), respectively, the gap between the testing coefficients of A and A' indicates that 83% of the stiffness reduction was considered and the other 17% was neglected in Model B. The reduction of the stiffness due to fire is greater than ex-

pected, and this difference can be attributed in part to the fire-induced

expected decrease in the concrete elasticity modulus, which cannot easily be accounted for in Model B.

η = calculated structural response in the considered section under the

testing load; $\mu\varepsilon$ = calculated structural response in the considered section under the service live load;μ = impact magnification factor.

The strain increments for each condition were measured under testing loads in the field test. The measured strains of section A′ are coincident with the theoretical strains, whereas the recorded strains of

Table 8
Deflection results from the tests (unit: mm).

Condition/Location	Load type	Gauge	Total value S_t	Elastic value S_e	Residual value S_p	Theoretical value S_S	Testing coefficient S_e/S_S	Relative residual S_p/S_t S%
Condition 1/Section A	eccentric	D1	−5.35	−5.29	−0.06	−5.12	1.03	1.12
		D2	−5.14	−5.07	−0.07	−4.79	1.06	1.32
		D3	−4.41	−4.38	−0.03	−4.46	0.98	0.68
	centered	D1	−4.94	−4.95	0.01	−4.81	1.03	−0.22
		D2	−5.14	−5.11	−0.03	−4.79	1.07	0.66
		D3	−4.87	−4.85	−0.02	−4.76	1.02	0.39
Condition 2/Section B	eccentric	D1	−4.87	−4.75	−0.10	−4.64	1.02	1.95
		D2	−4.57	−4.43	−0.12	−4.25	1.04	2.60
		D3	−4.14	−4.01	−0.12	−3.86	1.04	2.82
	centered	D1	−4.19	−4.25	0.03	−4.28	0.99	−0.72
		D2	−4.45	−4.46	0.00	−4.25	1.05	0.09
		D3	−4.50	−4.48	−0.02	−4.22	1.06	0.40
Condition 3/Section A′	eccentric	D1	−4.13	−3.88	−0.23	−4.72	0.82	5.55
		D2	−4.04	−3.84	−0.19	−4.43	0.87	4.65
		D3	−3.69	−3.61	−0.06	−4.13	0.87	1.60
	centered	D1	−3.89	−3.81	−0.07	−4.44	0.86	1.67
		D2	−3.95	−3.96	0.02	−4.43	0.89	−0.43
		D3	−3.77	−3.69	−0.07	−4.42	0.83	1.81

4

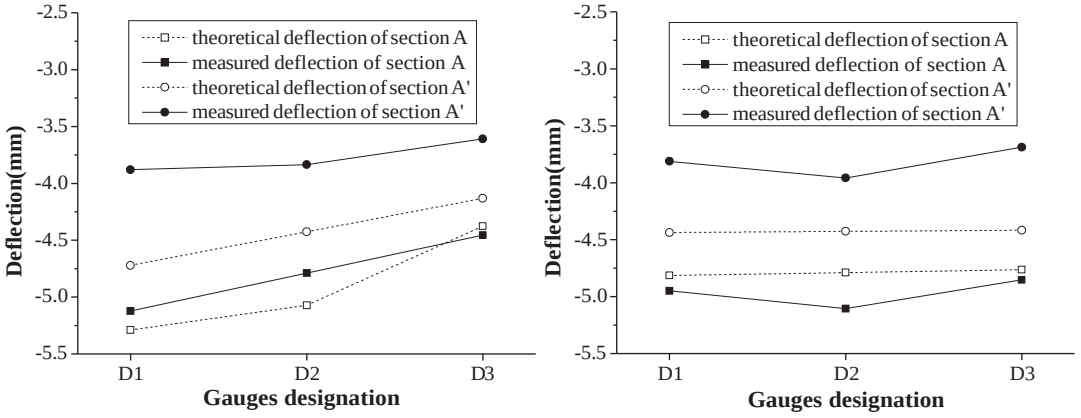

a) eccentric loads b) centered loads

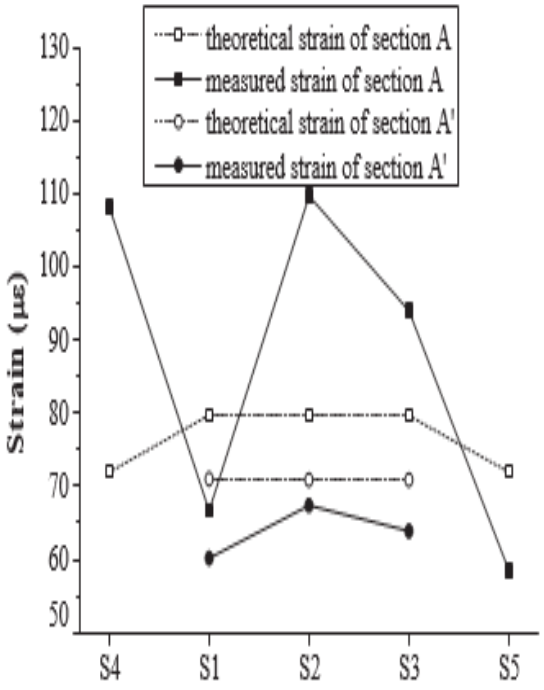

,

Fig. 23. Comparison of strains in sections A and A′.

sections A and B show wide dispersion due to the damaged interface for the strain gauges. Fig. 23 presents a comparison of the strains for sec- tions A and A′ under centered testing loads. In section A′, which was not

the testing coefficients of the strains varied from 0.76 to 0.95 under centered testing loads, which indicates that the strength of section A' can satisfy the design strength. However, in the postfire section A, the testing coefficients of the strains varied from 0.81 to 1.5. Therefore, the structural performances of the postfire spans are determined by the deflection results rather than by the strain results.

3.4. *DYNAMIC field test*

Using the DASP (data acquisition and signal processing) testing system, the dynamic characteristics of the postfire span 1 and non-affected span 1′ were measured using the ambient vibration test method [34]. The theoretical dynamic characteristics of Models A and B were analyzed with Midas software. The ambient acceleration data from span 1 are recorded in Fig. 24 a), and the frequency domain curve is ana-

lyzed in Fig. 24 b). Fig. 25 depicts the theoretical fundamental fre- quency (of 4.05 Hz) of the original Model A. According to the data of the dynamic characteristics from Table 9, both the measured funda- mental frequency and the theoretical fundamental frequency of span 1 were approximately 97% of those of span 1', indicating that the fire hazard had little influence on the frequency of the concrete structure in the fire scenario.

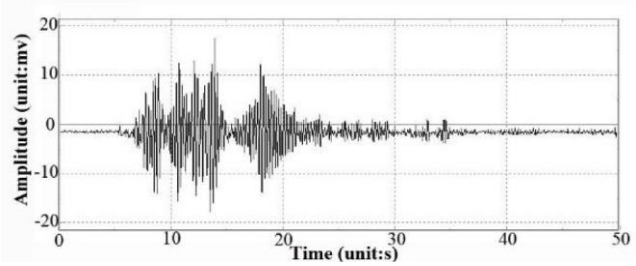

a) Ambient acceleration data

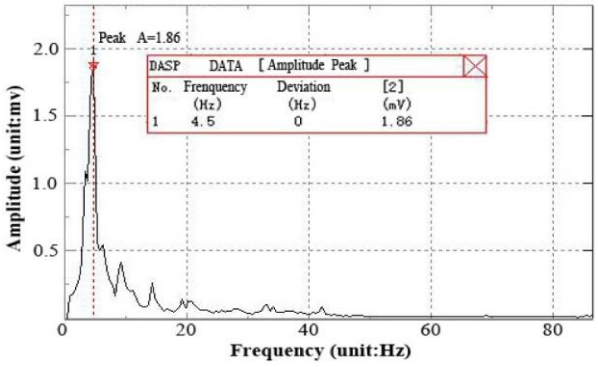

b) Frequency domain curve

Fig. 24. Field dynamic testing data.

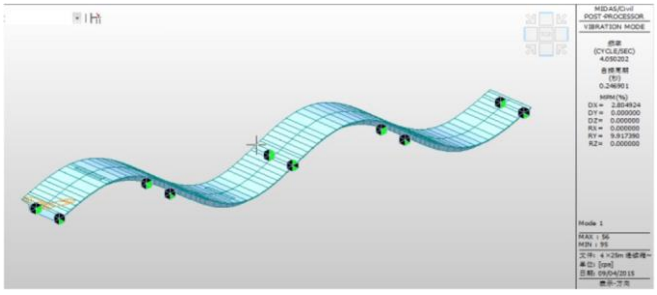

Fig. 25. Theoretical fundamental frequency in Model A.

3.5. The REPAIR of the S12 bridge

Based on all the investigations and analyses conducted, it was evi- dent that the mechanical properties of the materials of the S12 bridge were degraded. Furthermore, the residual loading capacity and stiffness of the S12 bridge were reduced and could not satisfy the design re- quirements. To restore the structural performance and enhance the durability and safety of the fired bridge, a set of repair measurements were determined and undertaken as follows: 1) the influenced surfaces of box beams and piers were flushed and cleaned; 2) spalling and de- laminated concrete were removed to depths of 2–8 cm according to the damage extent, exposed rebar was derusted by sand blasting and

Fig. 26. External prestressing strengthening at webs.

Fig. 27. Steel plate strengthening at the soffit.

Fig. 28. Coating with acrylic polyurethane paint.

broken sections were fixed with polymer mortar, including girders, abutment and piers; 3) the whole continuous unit 1 was strengthened by external prestressing with four strands fixed at lateral webs, as

Table 9
Comparison of the dynamic characteristics.

Test span	Model type	Measured fundamental frequency/Hz	Theoretical fundamental frequency/Hz	Measured damping ratio / %
Span 1	Model A	4.5	4.05	12.398
Span 1′	Model B	4.63	4.15	12.221

Fig. 29. Field loading test after repair.

depicted in Fig. 26; 4) steel plates were adhered at the soffit of boxes beams in spans 1 and 2, as shown in Fig. 27, and two layers of carbon fiber cloth were pasted over the plates; 5) the surfaces of beams in spans 1 and 2, abutment 0 and piers 1 and 2 were coated with acrylic poly- urethane paint (Fig. 27 and Fig. 28); and 6) all bearings were replaced in abutment 0 and piers 1 and 2. Subsequently, a field loading test was conducted after the repairs, as shown in Fig. 29, to determine the strengthening effect, and the repair was proven to be effective.

4. Conclusions

This paper presents the inspection, materials testing, field testing and parametric finite element analysis of a prestressed concrete box girder bridge after fire exposure. Subsequently, based on the in- vestigations and analysis, the repair requirements of the S12 bridge were determined and undertaken. The following conclusions can be drawn based on the results of the analysis:

1. After a detailed inspection, the following typical types of fire da- mage were observed: 1) concrete color changes with soot, pink and white-gray in the fire-affected area; 2) concrete spalling and cover loss in the soffit and web of the beam and pier columns; 3) map cracking in the beam and pier columns; and 4) reinforcing bar ex- posure in the deck.
2. According to the testing results of the concrete sampling cores taken from a depth of over 5 cm from the concrete surface, the compres- sive strengths of the postfire concrete retained approximately 93% and 96% of the room-temperature strength in the beam and pier, respectively. Additionally, the reduction coefficient of the yield strength of the postfire bar can be regarded as approximately 0.85, which indicates that the temperature of the testing bar reached 700 °C during the fire exposure. Based on the estimated temperature of the corrugated pipe during the fire exposure, the prestressing of the outmost N9 tendons conservatively retained 90% of the room-temperature prestressing. In addition, the temperatures at various depths of the S12 bridge elements were estimated according to the inspection results.
3. The deflection results obtained from the static proof load test in- dicate that the stiffness of span 1 decreased by approximately 23% after the fire exposure and can no longer satisfy the design re- quirement. The recorded strain increments of the postfire sections exhibited wide dispersion due to the damaged interface for the strain gauges. Therefore, the structural performances of the postfire spans are determined by the deflection results, rather than by the strain results.
4. According to the dynamic characteristic data, the measured funda- mental frequency of span 1 is approximately 97% of the original

fundamental frequency and the theoretical fundamental frequency. This result indicates that

the fire hazard had little influence on the frequency of the concrete structure.

5. The repair of the S12 bridge included surface treatment, rebar derusting, defects repair, external prestressing strengthening, steel plate and carbon fiber cloth reinforcement, coating and bearings replacement. Finally, a field loading test after the repairs was per- formed to determine the strengthening effect and proved the repairs to be effective.

References

1- X. Gong, A.K. Agrawal, Numerical simulation of fire damage to a long-span truss bridge, J. Bridge Eng. 20 (10) (2015) 04014109, https://doi.org/10.1061/(asce)be. 1943-5592.0000707.

2- B.F. Godart, J. Berthellemy, J.P. Lucas, Diagnosis, assessment and repair of the Mathilde bridge close to collapse during a fire, Struct. Eng. Int. 25 (3) (2015) 331–339, https://doi.org/10.2749/101686615X14210663188691.

3- G. Peris-Sayol, I. Paya-Zaforteza, S. Balasch-Parisi, J. Alós-Moya, Detailed analysis of the causes of bridge fires and their associated damage levels, J. Perform. Constr. Facil. 31 (3) (2017) 04016108, https://doi.org/10.1061/(asce)cf.1943-5509. 0000977.

4- M.Z. Naser, V.K.R. Kodur, A probabilistic assessment for classification of bridges against fire hazard, Fire Saf. J. 76 (2015) 65–73, https://doi.org/10.1016/j.firesaf. 2015.06.001.

5- X.G. Zhang, G. Liu, J.H. Ma, H.B. Wu, B.Y. Fu, Y. Gao, Status and prospect of technical development for bridges in China, Chin. Sci. Bull. 61 (2016) 415–425 https://doi.org/10.1360/N972015-00912.

6- L.J. Zhao, W.J. Li, M. F, Steel bridges development in China, China Highw. 11 (2016) 25–27.

7- Z.D. Lu, L. Su, The Chinese research progress on damage mechanism and evaluation method of concrete structure after fire in China, J. Build. Struct. S2 (2010) 202–209.

8- China Association for Engineering Construction Standardization(CECS), Standard Building Structural Assessment after Fire, CECS252, Beijing(China), 2009.

9- G.O. Shanafelt, W.B. Horn, Guidelines for Evaluation and Repair of Prestressed Concrete Bridge Members, NCHRP Report 280, Transportation Research Board, Washington, D.C.(USA), 1985.

10- A. Gustaferro, L.D. Martin, Design for Fire Resistance of Precast Prestressed Concrete, Prestressed Concrete Institute (PCI), Chicago, IL(USA), 1988.

11- Fib Working Party 4.3, State of the Art Report. Fire Design of Concrete Structures - Structural Behaviour and Assessment. Fib Bulletin 46, International Federation for Structural Concrete, Lausanne(Switzerland), 2008.

12- M. Garlock, I. Paya-Zaforteza, V. Kodur, L. Gu, Fire hazard in bridges: review, assessment and repair strategies, Eng. Struct. 35 (2012) 89–98, https://doi.org/10. 1016/j.engstruct.2011.11.002.

13- B. Georgali, P.E. Tsakiridis, Microstructure of fire-damaged concrete: a case study, Cement Concr. Compos. 27 (2) (2005) 255–259, https://doi.org/10.1016/j.

cemconcomp.2004.02.022.
14- N.R. Short, J.A. Purkiss, S.E. Guise, Assessment of fire damaged concrete using colour image analysis, Constr. Build. Mater. 15 (2001) 9–15, https://doi.org/10. 1016/s0950-0618(00)00065-9.
15- V.K. Kodur, A. Agrawal, Critical factors governing the residual response of re- inforced concrete beams exposed to fire, Fire Technol. 52 (2016) 967–993, https:// doi.org/10.1007/s10694-015-0527-5.
16- E. Aziz, V. Kodur, An approach for evaluating the residual strength of fire exposed bridge girders, J. Constr. Steel Res. 88 (2013) 34–42, https://doi.org/10.1016/j. jcsr.2013.04.007.
17- Z.D. Lu, J.F. Chai, J.T. Yu, A numerical approach for calculating the mechanical performance of the fire-damaged reinforced concrete continuous beams, J. Tongji
18- Univ. Nat. Sci. 75 (2012) 93–103, https://doi.org/10.11908/j.issn.0253-374x.2015.01.003.
19- Q. Huang, Inspection and evaluation of reinforced concrete bridges after fire dis-asters, World Bridg. 42 (5) (2014) 78–82.
20- Y. Guyon, Prestressed Concrete, F.J. Parsons, Limited of London, Folkestone and Hastings, London, 1953.
21- M. Davis, P. Tremel, A. Pedrego, Bill williams river concrete bridge fire damage assessment, Struct. Mag. 7 (2008) 30–32.
22- R. Stoddard, Inspection and Repair of a Fire Damaged Prestressed Girder Bridge, International Bridge Conference, Pittsburgh, 2004.
23- Z.D. Cai, X.M. Peng, Q. Huang, Inspection and assessment of concrete girder bridge damaged by fire, World Bridg. 42 (6) (2014) 74–78.
24- Q.W. Liu, C.M. Wang, W.L. Luo, Simulation analysis and evaluation of prestressed concrete hollow slab girder subjected to fire disaster, Highway 1 (2014) 35–43.
25- V.K.R. Kodur, L.A. Bisby, Evaluation of fire endurance of concrete slabs reinforced with fiber-reinforced polymer bars, J. Struct. Eng. 131 (1) (2005) 34–43, https:// doi.org/10.1061/(asce)0733-9445(2005) 131:1(34).
26- W.Z. Zheng, X.M. Hou, D.S. Shi, M.X. Xu, Experimental study on concrete spalling in prestressed slabs subjected to fire, Fire Saf. J. 45 (5) (2010) 283–297, https://doi. org/10.1016/j.firesaf.2010.06.001.
27- J. Alos-Moya, I. Paya-Zaforteza, M.E.M. Garlock, E. Loma-Ossorio, D. Schiffner,
A. Hospitaler, Analysis of bridge failure due to fire using computational fluid
28- dynamics and finite element models, Eng. Struct. 68 (6) (2014) 96–110, https://doi. org/10.1016/j.engstruct.2014.02.022.
29- Chang An University Engineering Center Inc (CHDEC), Special Detection Report of K61+479.541 Overpass Bridge after Fire. Report No.BG-2015-QL-JS-08, CHDEC, Xi an.(China), 2015.
30- M.S. Abrams, B. Erlin, Estimating post-fire strength and exposure temperature of prestressing steel by metallographic method, JPCA Res. 9 (3) (1967) 23–33, https:// doi.org/10.1145/321420.321438.
31- D.M. Glasheen, Petrographic

Examination of Hardened Concrete - WSDOT Bridge 509/11, Dominion Labs, Inc., Project No. S2084, 2003 March.

32- A. Gustaferro, L.D. Martin, Design for Fire Resistance of Precast Prestressed Concrete, Prestressed Concrete Institute (PCI), Chicago, IL (USA), 1988.

33- British Standard Institution. Eurocode 2: design of concrete structures- Part 1-2: general rules-Structural fire design, BS (Breed. Sci.) 1–2 (1992) 1992.

34- China Recommend Standard for Transportation (JTG/T). Load Test Methods for Highway bridge(China). JTG/T J21-01, (2015).

35- China Standard for Transportation (JTG), General Specifications for Design of Highway Bridges and culverts(China). JTG D60, (2015).

36- D.B. Ashebo, T.H.T. Chan, L. Yu, Evaluation of dynamic loads on a skew box girder continuous bridge Part I: field test and modal analysis, Eng. Struct. 29 (6) (2007) 1052–1063, https://doi.org/10.1016/j.engstruct.2006.07.014.